FORSCHUNGSZENTRUM JÜLICH GmbH

Institut für Plasmaphysik
Association EURATOM-KFA

Density Limits and Evolution of Disruptions on TEXTOR

G. Waidmann
G. Kuang

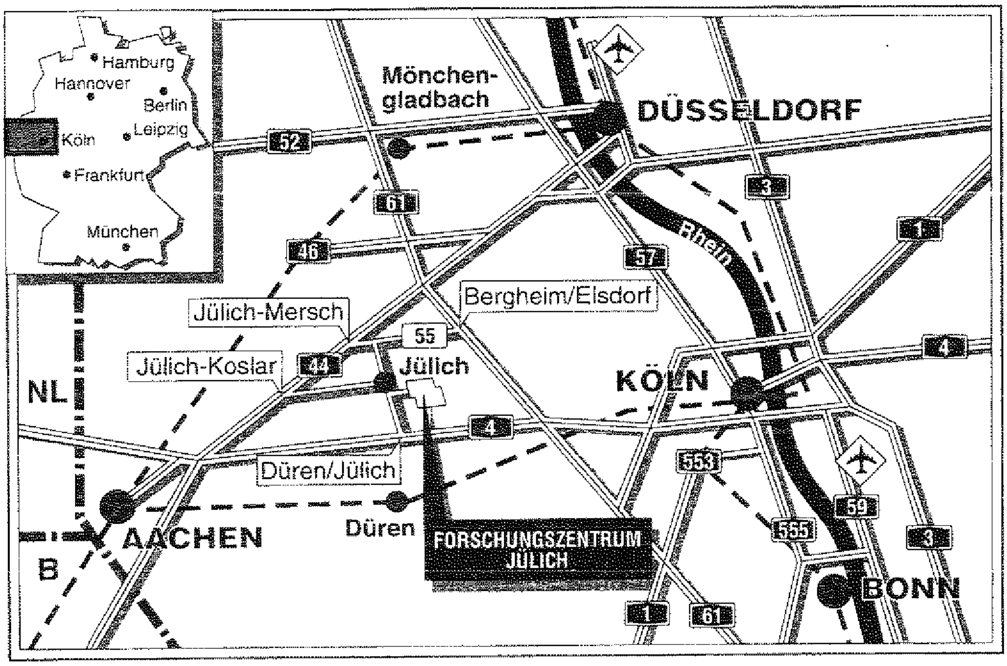

Berichte des Forschungszentrums Jülich ; 2448
ISSN 0366-0885
Institut für Plasmaphysik Jül-2448
Association EURATOM-KFA

Zu beziehen durch: Forschungszentrum Jülich GmbH · Zentralbibliothek
Postfach 1913 · D-5170 Jülich · Bundesrepublik Deutschland
Telefon: 02461/61-6102 · Telefax: 02461/61-6103 · Telex: 833556-70 kfa d

Density Limits and Evolution of Disruptions on TEXTOR

G. Waidmann
G. Kuang

DENSITY LIMITS AND EVOLUTION OF DISRUPTIONS ON TEXTOR

G. Waidmann, G. Kuang

Institut für Plasmaphysik, Forschungszentrum Jülich GmbH,

Association EURATOM-KFA, D-5170 Jülich, F.R.G.

ABSTRACT

Density limits and the evolution of disruptions were studied on TEXTOR for different wall materials facing the plasma surface. A systematic extension of the density limit was found over a large current range when the metallic wall was first exchanged by a carbon and later by a boron-carbon coated wall. The maximum attainable density nearly doubled when metallic impurities were replaced by low Z-impurities as boron and carbon. With a neutral beam additional heating power of P_{NI} = 3.2 MW average densities exceeding $\bar{n}_e = 10^{20}\ m^{-3}$ were obtained. The maximum density observed scales like the square root of the auxiliary heating power.

The sequence of processes leading to a density limit disruption has been experimentally analysed in detail for Ohmically heated plasmas. During the density increase in the gas feeding phase a boundary cooling by radiation and a steepening of the electron temperature gradient was observed. The plasma detaches from the limiters and MHD-activity is launched in the edge plasma. An $m=2$ mode in the outer plasma region coupled with an $m=1$ mode deeper in the plasma. During a first mode locking of the $m=2$ mode a strong heat pulse is emitted and a sharp increase of the impurity lines CV and OVI is found. The final energy quench is believed to be triggered by the overlapping of two coupled modes. The energy quench lasts in TEXTOR approximately 1 msec or less. The electron temperature profile evolution shows then a structure which could be interpreted as a filamentation of the plasma current. The decay of the plasma current after the energy quench is governed either by the resistance of the cold plasma or by the electric time constant of the TEXTOR liner.

1. INTRODUCTION

The density limit disruption is one of the critical processes which restrict the tokamak operation to a certain parameter range. Other limits are the q-limit or the electron run-away phenomenon at low electron densities. In the past a number of physical processes which influence the density limit /1-3/ were studied and described in the literature. More recently the ITER study group has brought new attention to this subject because of its importance for the future tokamak fusion programme. A collection of recent data appeared in ITER-physics R & D reports /4/.

In the TEXTOR programme /5/ the influence of wall materials and wall conditioning techniques for plasma facing components on the tokamak performance is investigated. In the first part of this paper we report new experimental data on density limits obtained for different exposed wall materials. A comparison for Ohmic and neutral beam heated plasmas is made and the dependence of the maximum density on auxiliary heating power is evaluated. In the second part we study physical processes leading to the major plasma disruption and show its time evolution.

The phenomenological picture of a density limit disruption for an Ohmically heated plasma is shown in Fig. 1. The average density $\overline{n}_e$ increases until a sudden break occurs. The central electron temperature on axis $T_e(Ro)$ oscillates because of normal sawtooth activity and falls on the average. In the very last phase the sawteeth stop and a temperature dip is seen before the final disruption takes place. The total radiation P_{Rad} shows an unusual behaviour. The radiative loss increases with density but suddenly the radiation power increases nonlinearly. At this time we observe in the plasma edge a luminous radiating ring and a separation of the edge plasma from the limiters.

2. THE OPERATIONAL REGIME OF TEXTOR

During the past years of operation different wall and limiter materials were exposed to the TEXTOR plasma. The maximum density obtainable in Ohmic discharges was found by continuous gas feeding. For a given plasma cross section the maximum density increased linearly with the plasma current up to a limiting current. The results are compiled in a

Hugill-diagram where the inverse safety factor $1/q_L^{cyl}$ is plotted against the normalized line averaged density $\bar{n}_e \cdot R/B_T$. For metallic walls (Inconell-liner; stainless steel limiters) a linear relation between $1/q_L^{cyl} \propto I_p$ and $\bar{n}_e \cdot R/B_T$ was found only up to a value $q_L \approx 3$. The lowest q-value that could be reached under these conditions was $q_L = 2.3$ /6/. The plasma was dominated by metallic impurities. A good progress was made by the carbonization technique /7/. The inner surface of TEXTOR was coated with an amorphous layer of carbon. The metal impurities were nearly completely excluded from the plasma now. The metal limiters were exchanged later against graphite limiters and the inner part of the liner was protected with graphite tiles (bumper limiter). A toroidal graphite belt limiter was installed in addition (ALT-pumping limiter). For the first time the theoretical limit $q_L = 2$ was reached. Over the whole current range the density limit was displaced to higher densities. The scatter of data indicates the different conditioning states encountered during various experimental phases. The main impurities found now were the low Z elements carbon and oxygen. The oxygen level was drastically lowered by the advent of the boronization technique /8/. Now the plasma facing components were covered with an amorphous film of boron plus carbon. A new impurity now was boron but the carbon content was reduced in addition by this new conditioning procedure. Again a clear shift of the density limit curve to higher values was found over the whole current range investigated. Z_{eff}-values around 1.1 were detected, but a plasma boundary cooling at the highest densities could not be avoided (Fig. 2).

With additional neutral beam heating this boundary heat loss can be supplemented and the density range can be expanded /9/. The density limits were studied with one injector delivering $P_{Co} = 1.7$ MW and with two injectors $P_{Co} + P_{Ctr} = 3.2$ MW. Average densities as high as $\bar{n}_e = 1.1 \times 10^{20}$ m^{-3} were measured. This corresponds to a normalized density $\bar{n}_e \cdot R/B_T \cdot q_L = 24.5$. The gas feeding was impeded by the formation of marfes on the high field side. The density limit was found to increase proportionally to the square root of the additional heating power delivered by the neutral beams but not like the total heating power.

The JET experiment obtained the highest densities after a beryllium coating of the inner surface with additional beam heating up to $P_{NI} = 20$ MW. For comparision, the highest densities they obtained came up to $\bar{n}_e = 1.4 \times 10^{20}$ m^{-3} /10/.

3. EVOLUTION OF A DENSITY LIMIT DISRUPTION

3.1 The T_e-profile contraction

With increasing average plasma density characteristic changes in the profile of electron density and temperature were observed. The radiative power loss mainly from impurities became always enhanced. At the time when the radiative loss P_{Rad} equals the Ohmic power input P_{OH} a typical change of the T_e-profile is observed. The edge temperature falls and the gradient of the electron temperature in the wings of the profile goes up (Fig. 3). The plasma detaches from the limiters. Such profile effects can be demonstrated by T_e-contour plots. Fig. 4 gives an example. Two time windows are shown for a discharge which ended with a density limit disruption. The 400 and 800 eV temperature lines have come closer to each other in the second, later contour plot. The T_e-profile has contracted and the plasma current density has changed its gradient with it. The plasma reacts with an instability as indicated by the T_e-oscillation visible in the second contour plot. Fig. 5 shows an ECE-signal from the temperature gradient regime of the plasma which contains information of active and passive MHD-phases in the forefront of a disruption. For our later discussion we have divided the time from the beginning of the first oscillation to the start of the major disruption into phases I, II and III.

3.2 MHD-activities

The ECE-diagnostics detect now in the edge plasma a periodic oscillation which was also magnetically observed by a resonant m = 2 coil system /11/. Two conjugate ECE-channels show the same growing oscillation at a radial position which is close to the expected q = 2 surface of this current profile. The oscillation amplitude saturates and the oscillation suddenly stops (Fig. 6a). A mode locking process is seen here. The important role of mode locking on density limit disruptions was discussed in the literature /12-14/. After mode locking the amplituede of the detected mode signal decays slowly. A growth time constant for $\tilde{T}_e$ of the m = 2 mode was evaluated here by the ECE-measurement to $\gamma_{m=2}^{-1}$ = 1.5 msec. A steep heat pulse was observed in the outermost ECE-channels after the locking occurred (Fig. 7) and the global plasma energy began to drop. One source region for the emitted heat pulse was found as a deep dip in two ECE-channels on the high field side in the steep T_e-gradient region. This event is accompanied by a sharp increase of the impurity line radiation of CV and OVI (Fig. 14).

Deeper in the plasma another oscillation begins to grow (Fig. 6b). Its amplitude reaches large values only later when the outer mode has locked already. A cross-correlation analysis determines this mode as an $m=1$ mode. The signature of the inner $m=1$ mode is later sometimes found on those ECE-signals which showed before locking the $m=2$ even mode, i.e. on the $q=2$ surface. A mode coupling is recognized here by this observation /22/. The electron temperature $\tilde{T}_e$ of the inner mode grows with a time constant $\gamma_{m=1}^{-1}$ = 3-4 msec. The frequency spectra of the two modes observed are not identical but show the same fundamental frequency (Fig. 8). Fig. 9 gives an example of mode coupling during the evolution towards a major density limit disruption. The oscillating motion of the inner mode disappears abruptly after a few periods on the high field side of the plasma and a rapid temperature drop is observed. The electron temperature profiles obtained from ECE clearly reflect a dynamic behaviour introduced by the MHD activity. Two shoulders are seen in the edge plasma after $m=2$ mode locking. The locked mode flattens over a certain radial range the T_e-gradient in the T_e-profile. In the central plasma, close to the sawtooth inversion radius, a relative T_e-minimum developed later as a consequence of the inner mode coupling with the $m=2$ mode. Fig. 10 shows for a comparison the T_e-profile at a time before the MHD-mode activity began and at the end of phase I.

This situation now could lead to the final energy quench. In this shot (#43121) however a delay was brought about by the unlocking of the modes. Both modes begin to rotate again. The distorted T_e-profile partially recovers. The $m=2$ shoulders disappear and the T_e-dip is reduced for a transient time span (Fig. 11). The modes however show a very nonsinusoidal oscillation now until a second mode locking occurs.

3.3 The energy quench

At the end of phase II the $m=2$ mode has reached a large amplitude again but stops rotating soon. The oscillation of the inner mode shows a more complicated structure. The cross-correlation analysis suggests a 3/2-mode now. A broadening of the central T_e-profile is observed when the inner mode stops (phase III). The T_e-profile is shown in Fig. 12. A slight temperature trough develops then. From the T-10 experiment /15/ a hollow soft x-ray emissivity profile was reported at the start of the energy quench. This can be understood by the radiative loss from the central plasma. A bolometric measurement demonstrates in this phase a developing strong radiation peak in the plasma center. On the high field side of the T_e-profile we observe again the m = 2 shoulder and deeper in the plasma a temperature step approximately at the q = 1.5 rational surface.

We believe the overlap of two magnetic islands leads now to a stochastisation of the magnetic field lines. Already in the year 1966 Rosenbluth et al. /16/ pointed out the possibility of a destruction of flux surfaces when resonances overlap. Later numerical simulations /17-19/ of the nonlinear interaction of tearing modes demonstrated that the m = 2, n = 1 mode destabilizes other modes on a rapid time scale. Because of the development of magnetic islands which overlap after an evolution time magnetic field lines become stochastic in a sizable part of the plasma cross section. In TEXTOR the decay of the kinetic plasma energy then occurs in 1 msec or sometimes even in a shorter time. The energy loss is fastest on the low field side of the plasma. Fig. 13 shows the T_e-profile development during the energy quench. A structure is seen during the energy decay process which could be interpreted as a current filament formation. In a numerical MHD modelling of the density limit disruption by Bondeson et al. /19/ such a filamentation process was indeed observed. The m = 2 pedestal on the high field side of the profile was observable up to the latest phase of the energy quench. Fig. 14 shows the appearance of impurity lines with respect to the m = 2 mode locking and the final energy quench.

3.4 The current decay phase

After the energy quench a last phase of the discharge is indicated in Fig. 14 by the enhanced emission of carbon and oxygen impurity lines. A small positive pip on the current curve signals the begin of the current decay. A negative voltage spike is observed during the final energy quench. The negative voltage spike has negative precursors which show up already during the growth of the MHD-modes. These voltage signals (Fig. 15) are interpreted as changes of the current profile. The observed deformations of the T_e-profile suggest this interpretation. During the current decay however a positive loop voltage was registered which led to a transient megawatt heating of the polluted cold plasma. A proper shutdown of the primary currents in the rectifier circuit prevents the formation of a lasting run-away current. Different current decay times were found. An exponential decay with a time constant τ_{Ip} = 14 msec was recorded when the plasma current decayed in the bulk plasma (Fig. 15). From this time constant one estimates an average electron temperature in the early decay of $T_e \approx 20$ eV. The time constant gets shortened if one adds intentionally gas impurities. The temperature then comes down to $T_e \approx 10$ eV. A short time constant τ_{Ip} = 3 msec was sometimes observed. It was found when the plasma position was lost by the position feedback system and the plasma current was transferred into the liner of TEXTOR. The liner L/R-time was calculated to $\tau_L \approx 3$ msec.

4. SUMMARY

The accessible density range for the operation of TEXTOR was steadily enlarged by reducing the impurity content of the plasma, i.e. by lowering of the effective Z. The q=2 limit was reached after removal of the metallic impurities. The density limit increases linearly with the plasma current. Deviations were observed when approaching the q-limit. Auxiliary heating by neutral beams increased the density limit proportional to the square root of the neutral beam power. Average densities above 10^{20} m^{-3} were obtained. The occurrance of marfes observed on the high field side of the plasma boundary impeded the gas feeding of the discharge during beam heating. It prevented the operation at possibly still higher densities.

The time evolution of the density limit disruption was studied in detail for Ohmic discharges. Radiative boundary cooling /20-21/ steepened the electron temperature gradient of the T_e-profile and destabilized MHD-modes primarily in the edge plasma. The locking of an m=2 mode resulted in the emission of a steep heat pulse and in the influx of light impurities as carbon, oxygen and boron. A mode coupling of m=2 with an inner mode m=1 or m=3/2 was observed. The overlap of inner and outer magnetic islands is believed to bring about the rapid energy quench which takes place in TEXTOR in approximately 1 msec. The unlocking of modes can delay the final energy quench for a short time. A strong radiative power loss from light impurities was observed during the energy quench phase and during the current decay. The long time constant of the bolometric detection system did not allow a quantitative measurement during the rapid energy decay. The current decays in the last phase of the discharge with a time constant which is either determined by the resistance of the cold, polluted plasma or by the electric time constant of the TEXTOR liner. The study described here will be continued by a systematic investigation of the disruption phenomena in plasmas with high power of additional heating.

ACKNOWLEDGEMENT

The authors would like to thank the TEXTOR-operation, the beam-heating and the data-acquisition teams for their work.

5. REFERENCES

/1/ Murakami, M., Callen, J.D. et al., Nucl. Fusion 16, (1976) 347

/2/ Stott, P.E., Hugill, J. et al., Controlled Fusion and Plasma Physics, 8th EPS Conf. Prague (1979) Vol. 1, 151

/3/ Greenwald, M., Terry, J.L. et al., Nucl. Fusion 28, 12 (1988) 2199

/4/ ITER Physics R & D Reports, ITER-TN-PH-9-7/PH17 (1989)
ITER-TN-PH-0-3/PH17 (1990)

/5/ Wolf, G.H. et al., Plasma Physics and Controlled Nucl. Fusion, 28 No. 9 (1986) 1413

/6/ Waidmann, G. et al., Plasma Physics and Controlled Nucl. Fusion, Vol. I (1984) 193

/7/ Waelbroeck, F. et al., J. Nucl. Mat. 121 (1984) 378

/8/ Winter, J. et al., Proc. 8th Int. Conf. on Plasma Surface Interactions in Controlled Fusion Devices, Jülich, May 1988, 713

/9/ Hugill, J. et al., Report CLM-R 239 (1983)

/10/ Keilhacker, M. et al., Report JET-P(89) 83

/11/ Waidmann, G. et al., EC-7 Workshop on ECE and ECR-Heating, P.R. China (1989), 92.
Plasma Physics and Controlled Fusion 31, No. 3 (1989) 323

/12/ Jensen, T.H., Chu, M.S., J. Plasma Phys. 30 (1985) 57

/13/ Persson, M., Bondeson, A., Nucl. Fusion 29, No. 6 (1989) 989

/14/ Wesson, J.A. et al., Nucl. Fusion 29, No. 4 (1989) 641

/15/ Kislov, D.A. et al., Controlled Fusion and Plasma Heating, 17th EPS Conf. Amsterdam (1990) Vol. 14B, Part I, 315

/16/ Rosenbluth, M.N. et al., Nucl. Fusion 6 (1966) 297

/17/ Carreras, B. et al., Phys. Fluids 23 (1980) 1811

/18/ Turner, M.F., Wesson, J.A., Nucl. Fusion 22, No. 8 (1982) 1069

/19/ Bondeson, A., Parker, R., submitted to Nucl. Fusion

/20/ Gibson, A., Nucl. Fusion 16 (1976) 546

/21/ Campbell, D.J. et al., 11th Conf. on Plasma Physics and Controlled Nucl. Fusion Research, Kyoto, Vol. I (1986) 433

/22/ Bussac, M.N. et al., 6th Conf. on Plasma Physics and Controlled Nucl. Fusion Research, Berchtesgaden, Vol. I (1976) 607

6. FIGURE CAPTIONS

Fig. 1 Typical signals of the line averaged electron density $\bar{n}_e$, the electron temperature on axis $T_e(R_o)$ and the total radiated power P_{Rad} from an Ohmic discharge which disrupted at the density limit at the time t = 1.418 sec.

Fig. 2 The operational regime of TEXTOR for different wall conditions. The curves labelled OH represent Ohmic discharges; NBI indicates neutral beam heated plasmas.

Fig. 3a-b Begin of an electron density- (a) and temperature-profile (b) contraction. A plasma detachment from the limiters became visible then in a CCD-camera recording.

Fig. 4 T_e-contour plot for two time windows in a discharge which disrupted at t = 1.837 sec at the density limit. The 400 eV and 800 eV contour lines come closer to each other in the later time window, demonstrating an increase in the T_e-gradient. The late temperature oscillation in the edge plasma signals MHD-activity.

Fig. 5 An ECE-signal from the T_e-gradient region which exhibits a sudden burst of MHD-activity. The different rotating and locked mode sequences are labelled phase I, II, and III.

Fig. 6a Two ECE-signals from the edge plasma show a growing m = 2 mode in phase I. (EC1 from LFS; EC10 from HFS). The mode locking phase is marked. A growth time constant is found $\gamma_{m=2}^{-1}$ = 1.5 msec.

Fig. 6b In the lower part of the figure an inner mode m = 1 develops slower and reaches its full amplitude when the m = 2 mode has stopped already. The two conjugate signals EC7 and EC8 have now a phase shift of $\Delta\varphi$ = 180°.

Fig. 7a-b Heat pulses leaving the plasma after m = 2 mode locking. They are detected here in the radially outermost ECE-channels on high (HFS) and low field side (LFS) of the plasma profile.

Fig. 8a-b Frequency spectra of the m = 2 mode (upper curve) and of the m = 1 mode (lower curve).

Fig. 9 Example of a mode coupling between m = 2 (signals EC9, EC10) and m = 1 mode (signals EC7, EC8).

Fig. 10 Comparison of the T_e-profile before the onset of MHD-activity t_b and at the end t_e of the phase I mode locking.

Fig. 11 T_e-profiles during mode unlocking in phase II.

Fig. 12 T_e-profile at the end of phase II. The $m=2$ mode has locked again. The central T_e-profile has broadened and a slight trough is observed.

Fig. 13 T_e-profile evolution during the energy quench. A radial structure is always observed during the fast energy decay.

Fig. 14 The sudden increase of impurity lines as CV and OVI is shown at the events of mode locking, energy quench and during the current decay.

Fig. 15 Time dependence of current I_p and loop voltage U_{Loop} during the current decay phase. The first observation of MHD-modes, the event of a first mode locking and the energy quench time are marked.

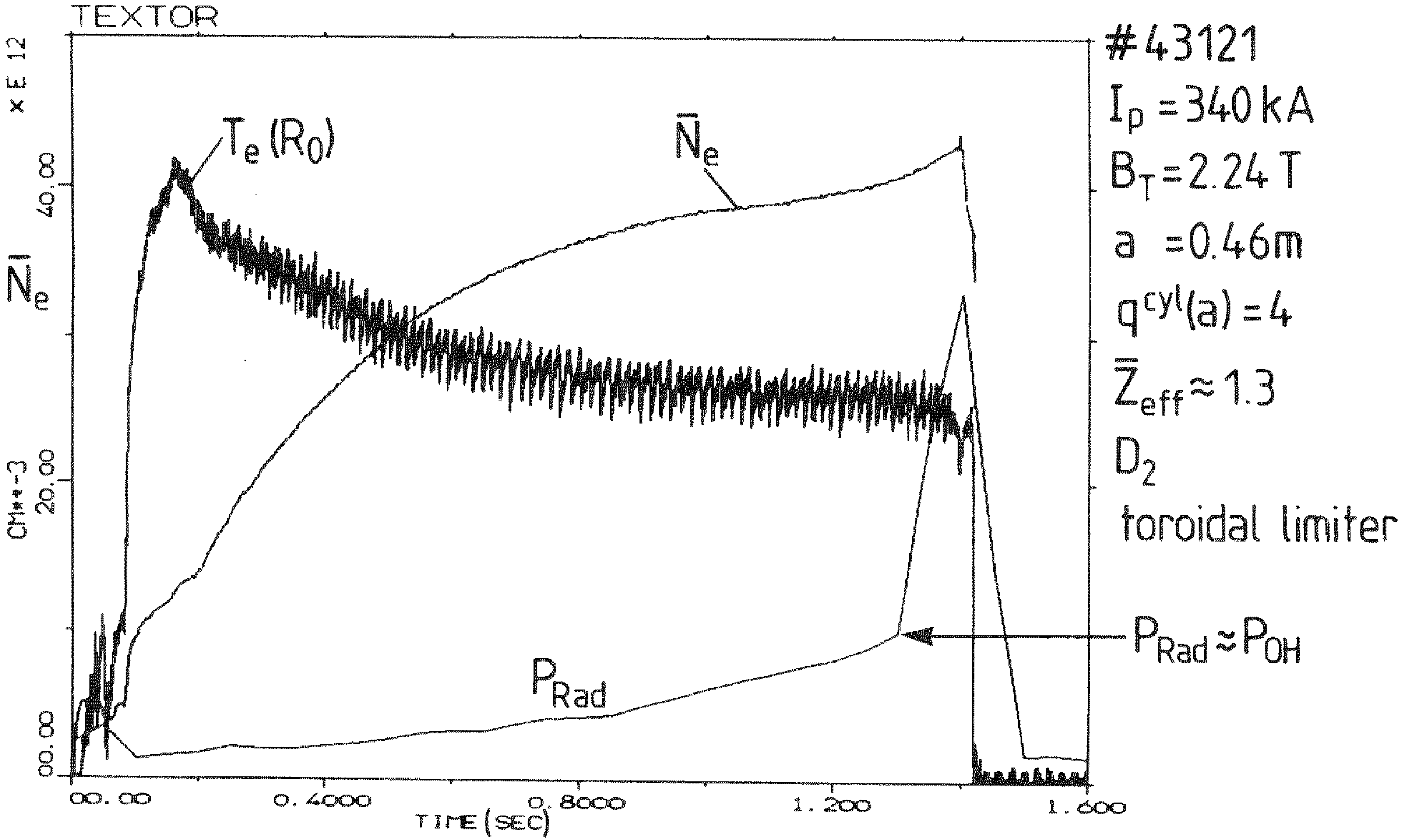

TEXTOR
× E 12
$\bar{N}_e$
CM**-3
40.00
20.00
00.00
$T_e(R_0)$
$\bar{N}_e$
P_{Rad}
00.00
0.4000
0.8000
1.200
1.600
TIME (SEC)
#43121
I_p = 340 kA
B_T = 2.24 T
a = 0.46m
$q^{cyl}(a)$ = 4
$\bar{Z}_{eff} \approx 1.3$
D_2
toroidal limiter
$P_{Rad} \approx P_{OH}$

Fig. 1

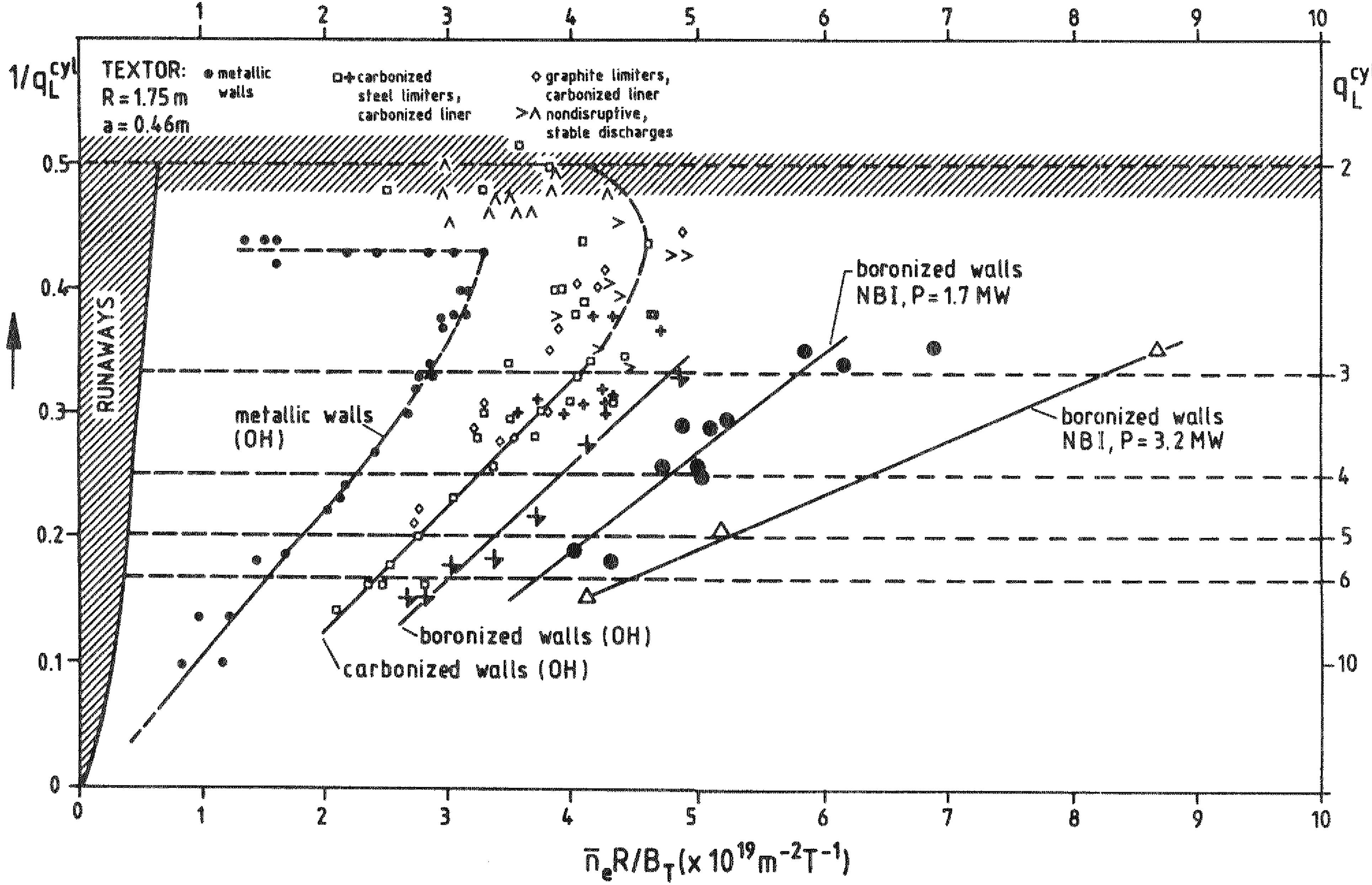

TEXTOR:
R = 1.75 m
a = 0.46m
metallic walls
carbonized steel limiters, carbonized liner
graphite limiters, carbonized liner
nondisruptive, stable discharges
RUNAWAYS
metallic walls (OH)
boronized walls (OH)
carbonized walls (OH)
boronized walls NBI, P = 1.7 MW
boronized walls NBI, P = 3.2 MW
$1/q_L^{cyl}$
q_L^{cyl}
$\bar{n}_e R/B_T (\times 10^{19} m^{-2} T^{-1})$

Fig. 2

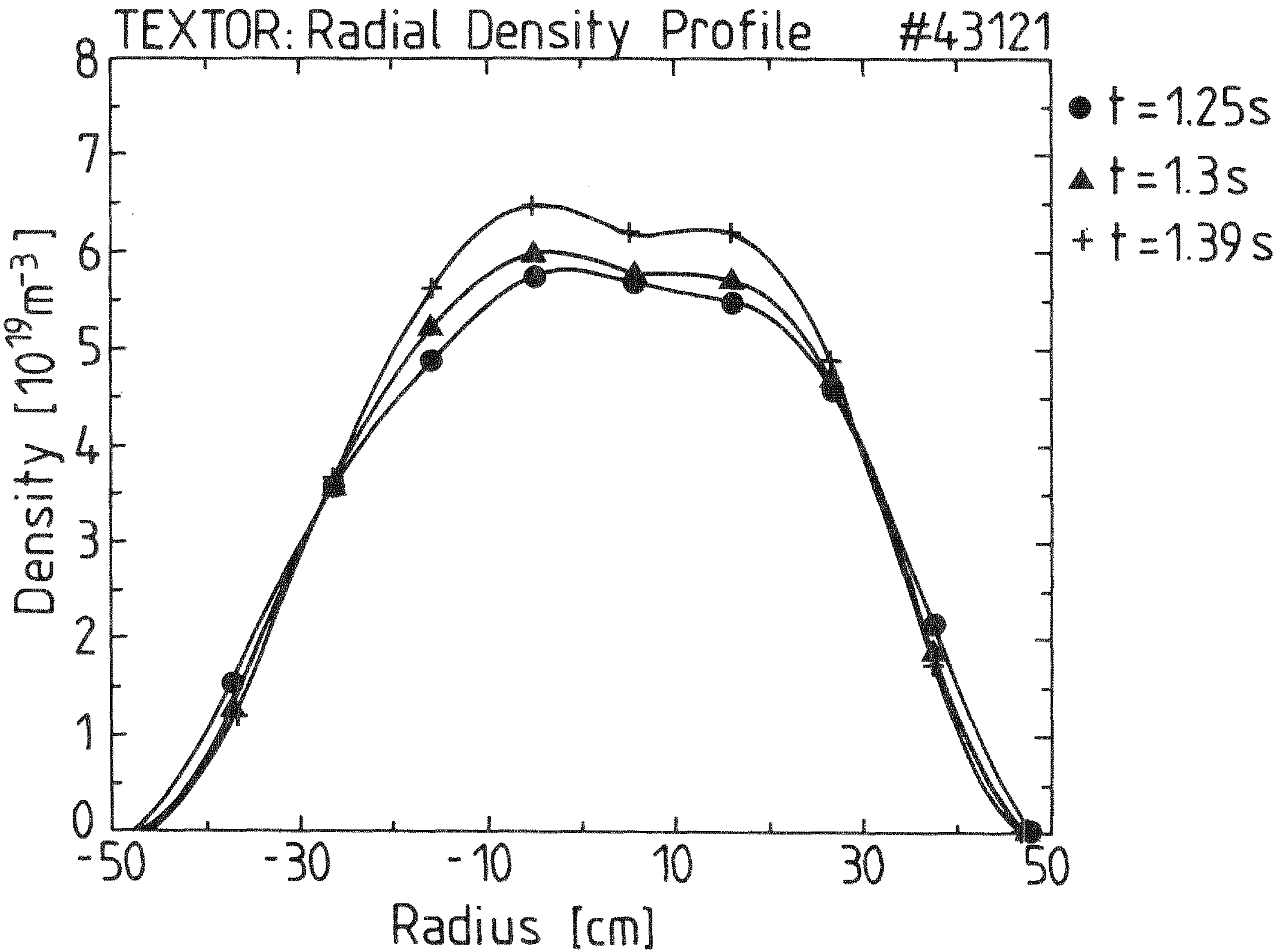
TEXTOR: Radial Density Profile #43121
Density [$10^{19}m^{-3}$]
Radius [cm]
0
1
2
3
4
5
6
7
8
-50
-30
-10
10
30
50
● t = 1.25s
▲ t = 1.3s
+ t = 1.39 s

Fig. 3a

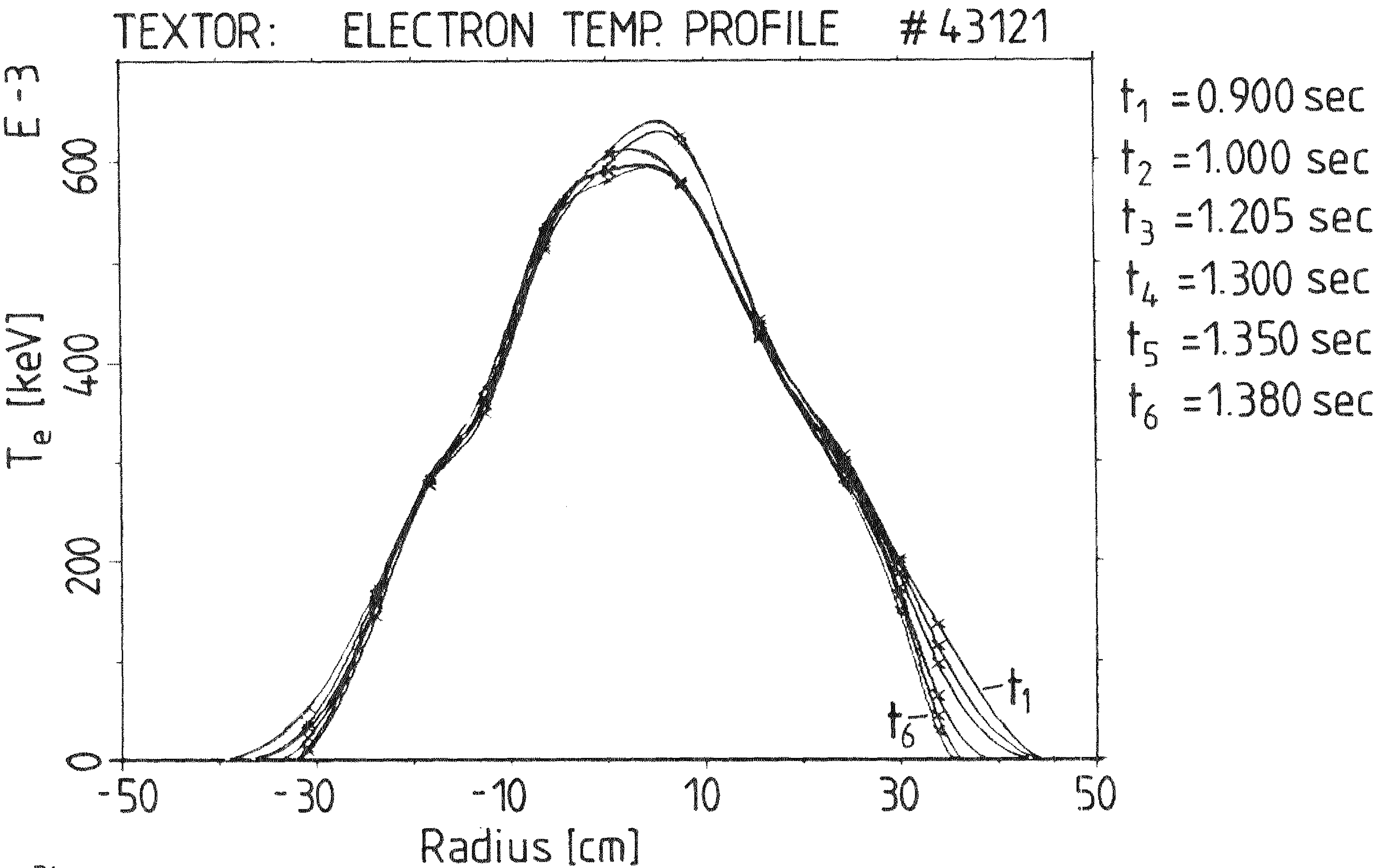
TEXTOR: ELECTRON TEMP. PROFILE #43121
E -3
Te [keV]
600
400
200
0
-50
-30
-10
10
30
50
Radius [cm]
t1 =0.900 sec
t2 =1.000 sec
t3 =1.205 sec
t4 =1.300 sec
t5 =1.350 sec
t6 =1.380 sec
t1
t6

Fig. 3b

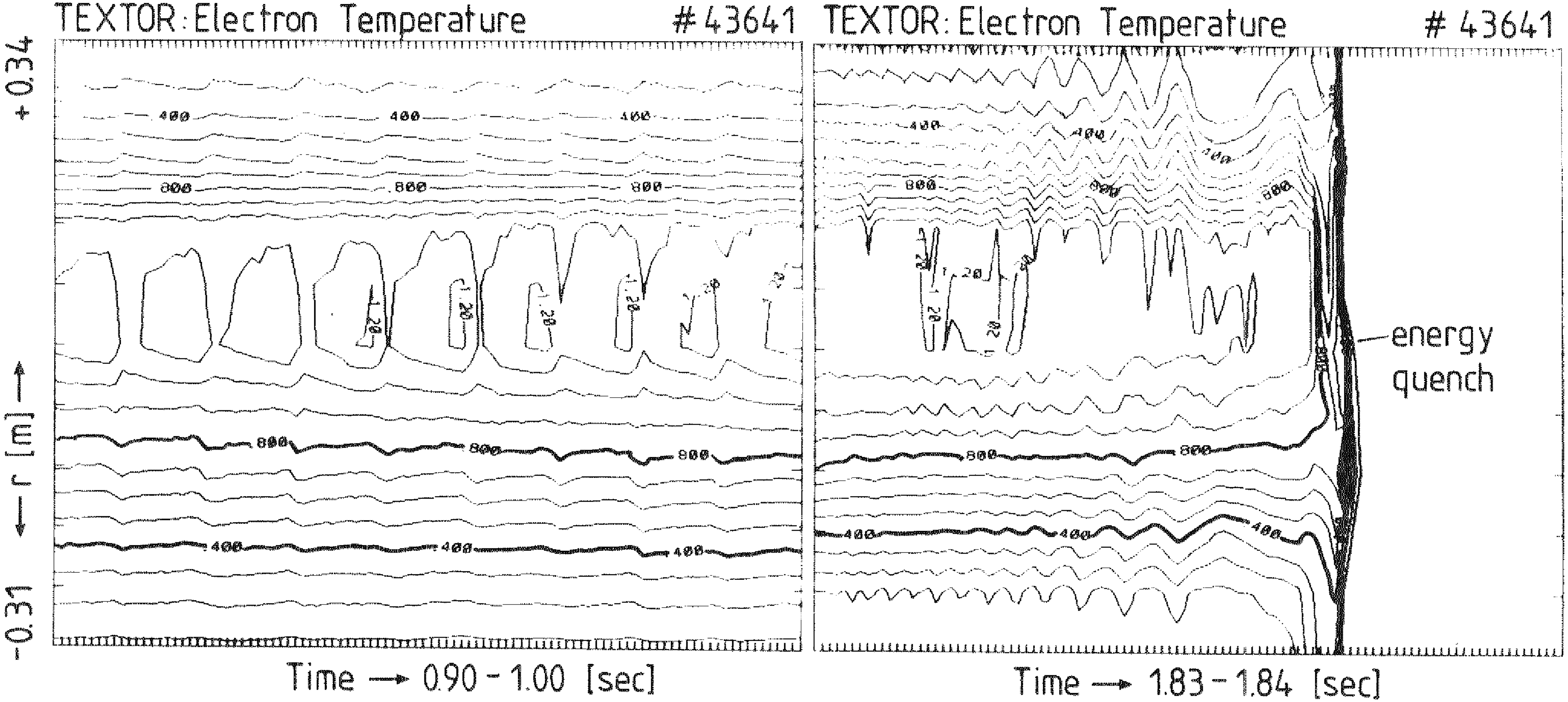
TEXTOR: Electron Temperature
43641
TEXTOR: Electron Temperature
43641
+0.34
-0.31
← r [m] →
energy quench
Time → 0.90 - 1.00 [sec]
Time → 1.83 - 1.84 [sec]

Fig. 4

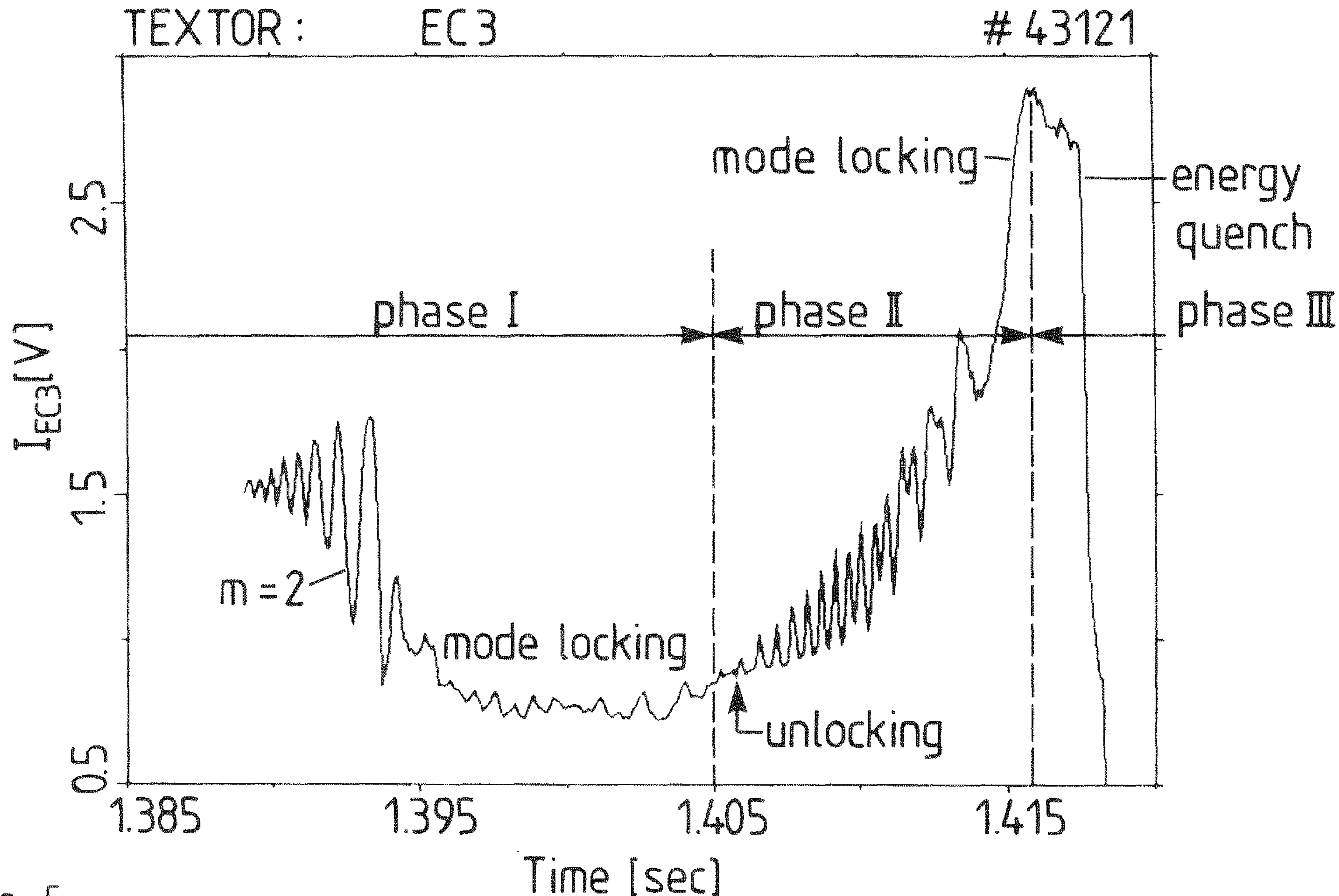
TEXTOR : EC3 # 43121
mode locking
energy quench
phase I
phase II
phase III
m = 2
mode locking
unlocking
I_{EC3} [V]
2.5
1.5
0.5
1.385
1.395
1.405
1.415
Time [sec]

Fig. 5

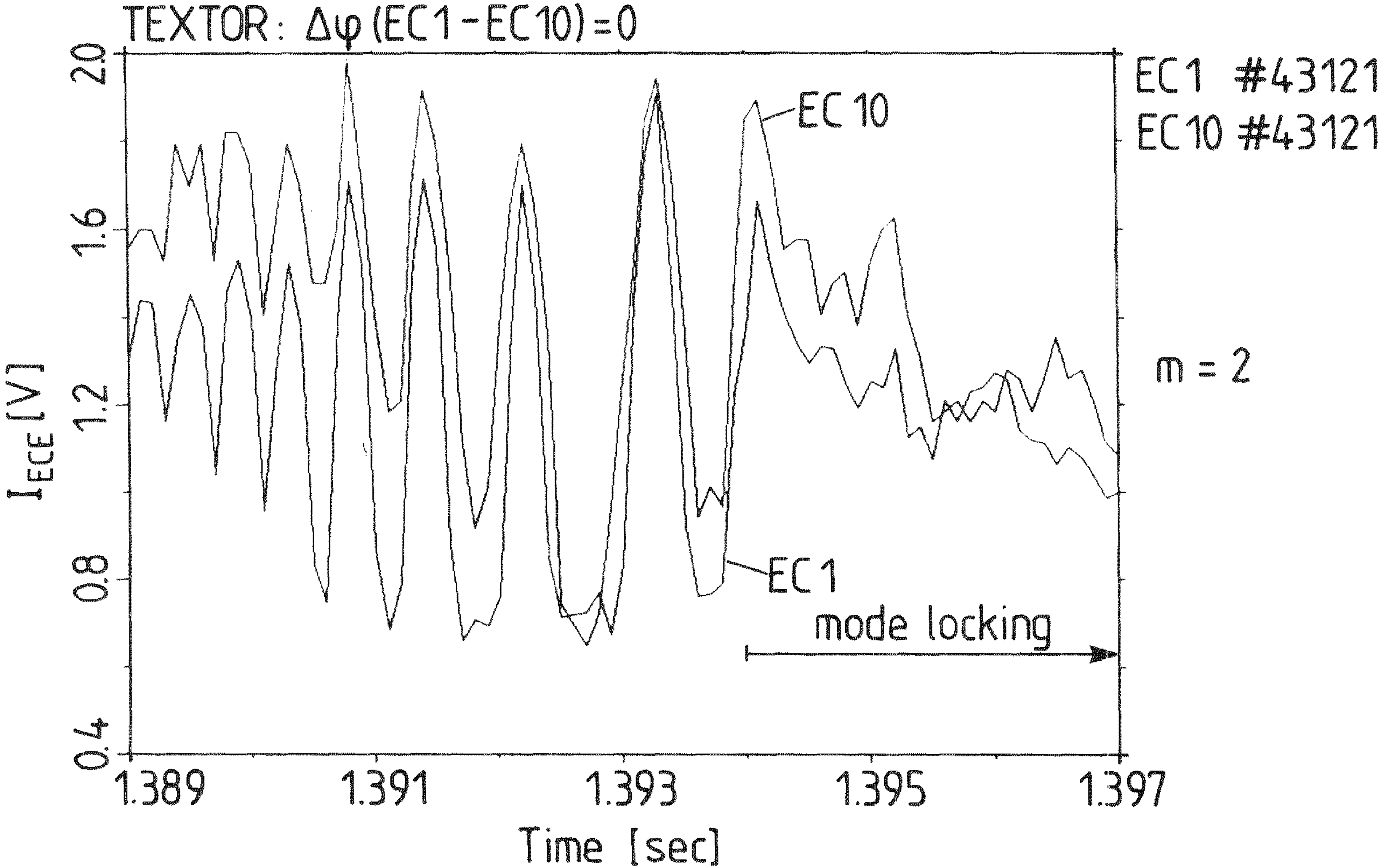
TEXTOR: Δφ (EC1 − EC10) = 0
EC1 #43121
EC10 #43121
EC10
EC1
m = 2
mode locking
I_ECE [V]
2.0
1.6
1.2
0.8
0.4
1.389
1.391
1.393
1.395
1.397
Time [sec]

Fig. 6a

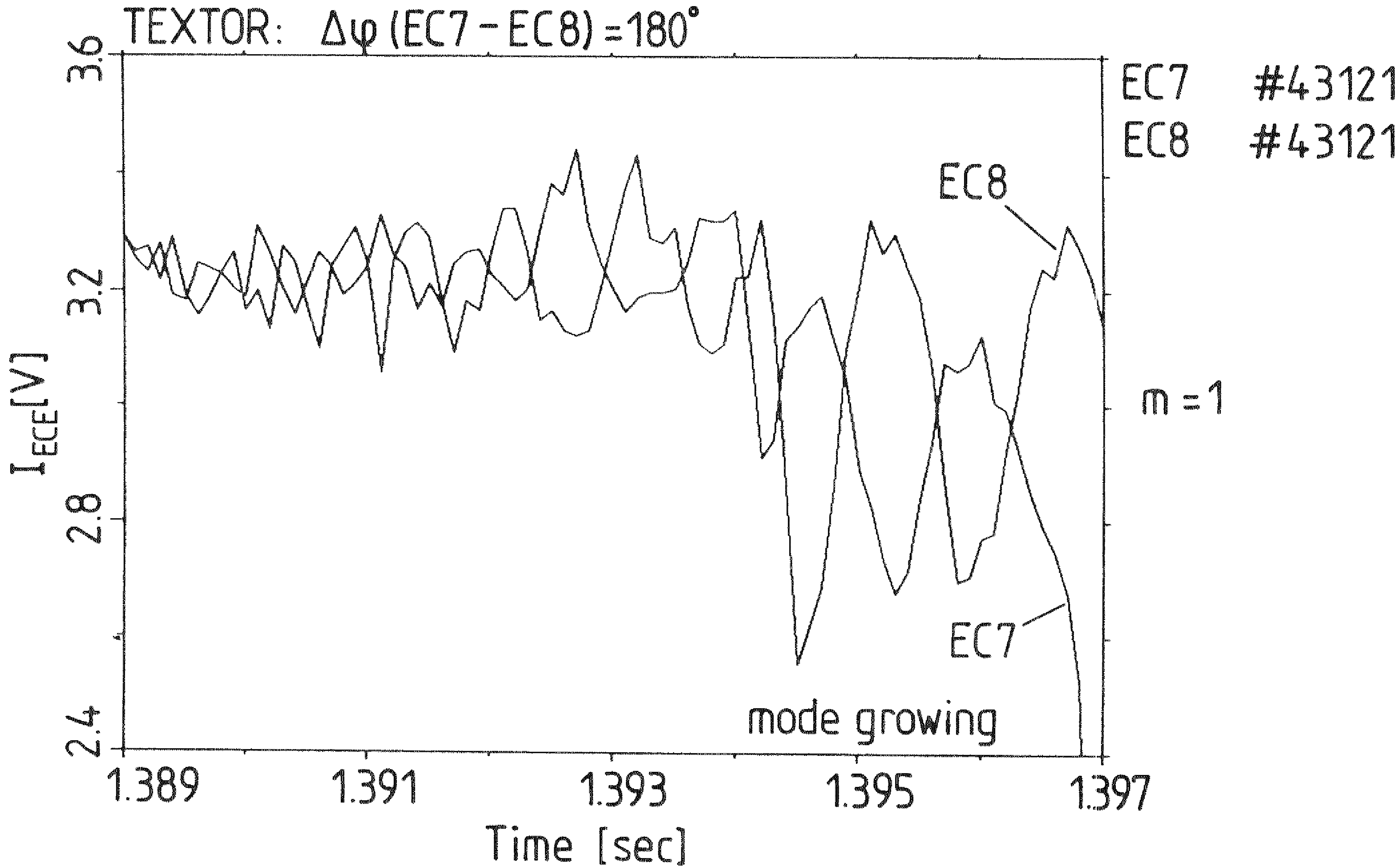
TEXTOR: Δφ (EC7 – EC8) = 180°
EC7 #43121
EC8 #43121
EC8
m = 1
EC7
mode growing
3.6
3.2
2.8
2.4
I_ECE [V]
1.389
1.391
1.393
1.395
1.397
Time [sec]

Fig. 6b

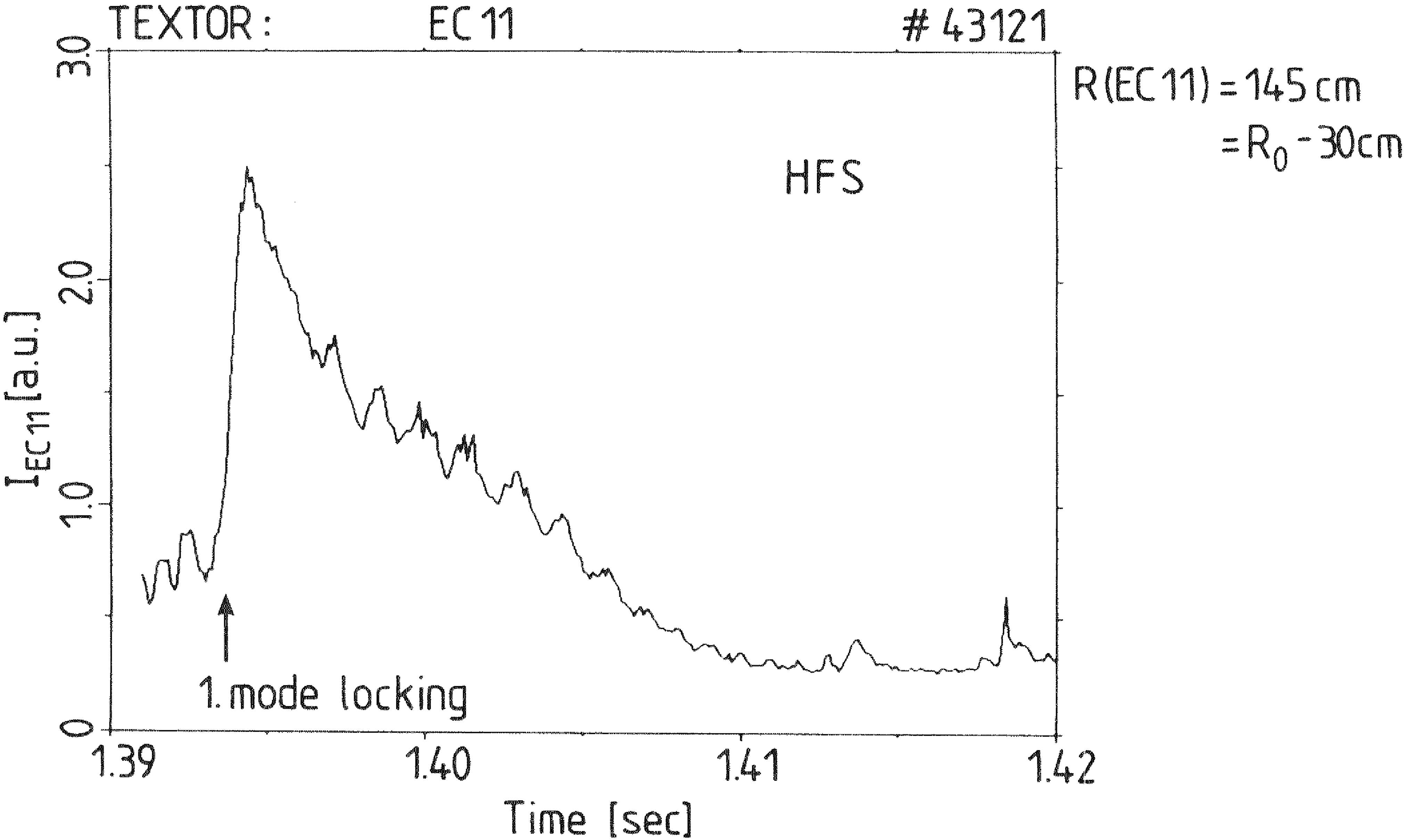
TEXTOR:
EC 11
43121
R(EC11) = 145 cm
= R0 - 30cm
HFS
I EC11 [a.u.]
3.0
2.0
1.0
0
1. mode locking
1.39
1.40
1.41
1.42
Time [sec]

Fig. 7a

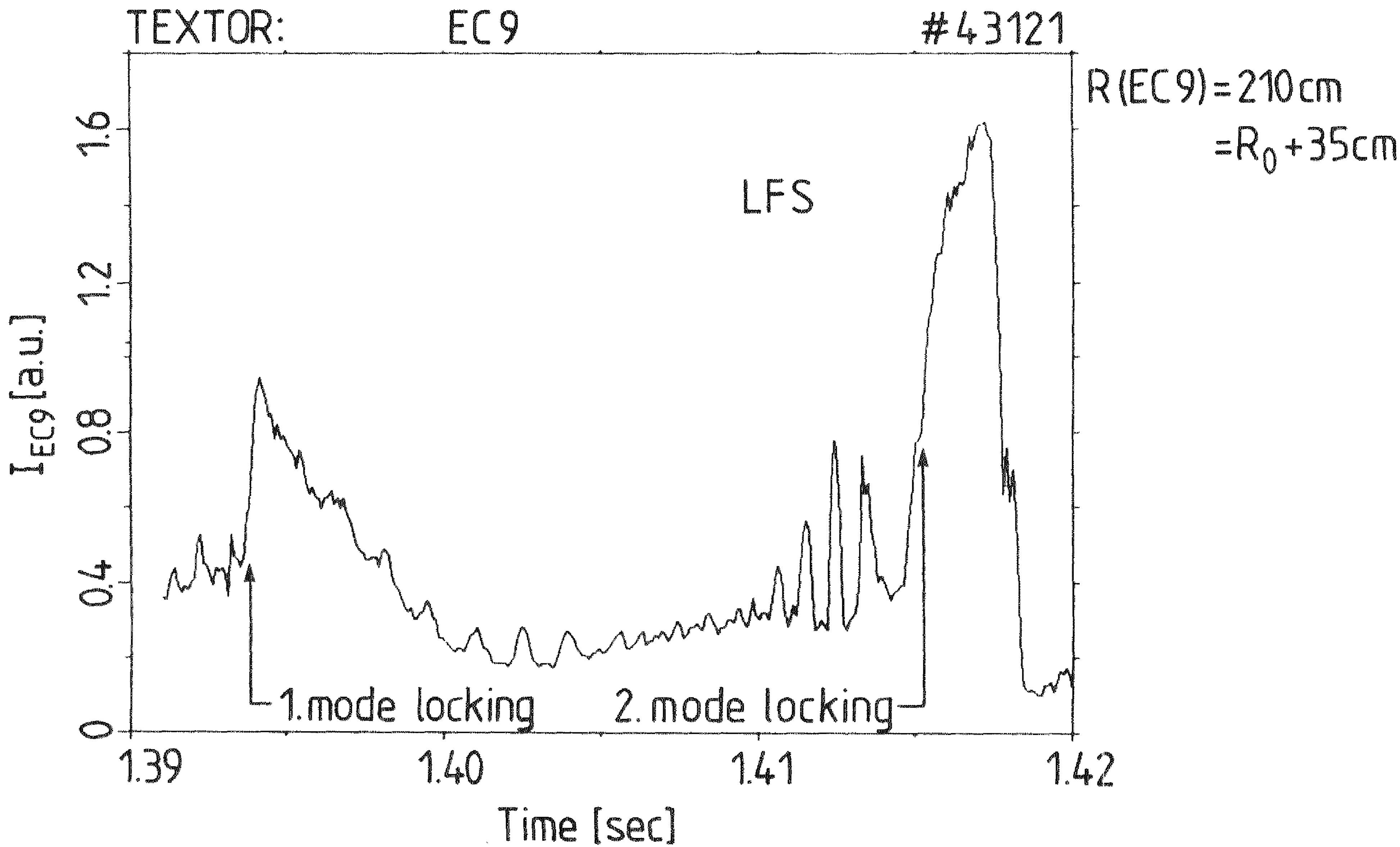
TEXTOR:
EC9
#43121
R(EC9) = 210 cm
= R_0 + 35 cm
LFS
I_{EC9} [a.u.]
1.6
1.2
0.8
0.4
0
1.mode locking
2. mode locking
1.39
1.40
1.41
1.42
Time [sec]

Fig. 7b

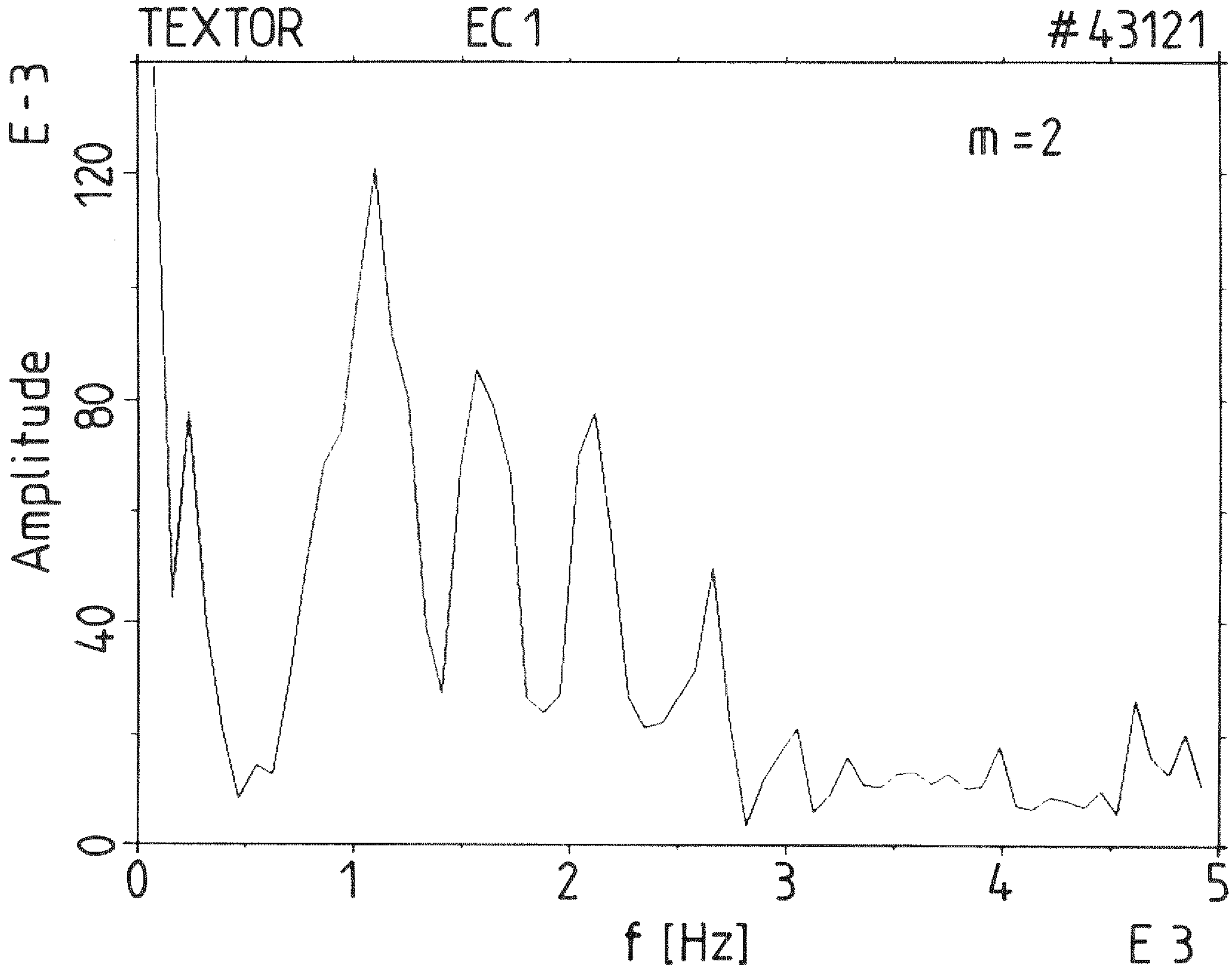

Fig. 8a

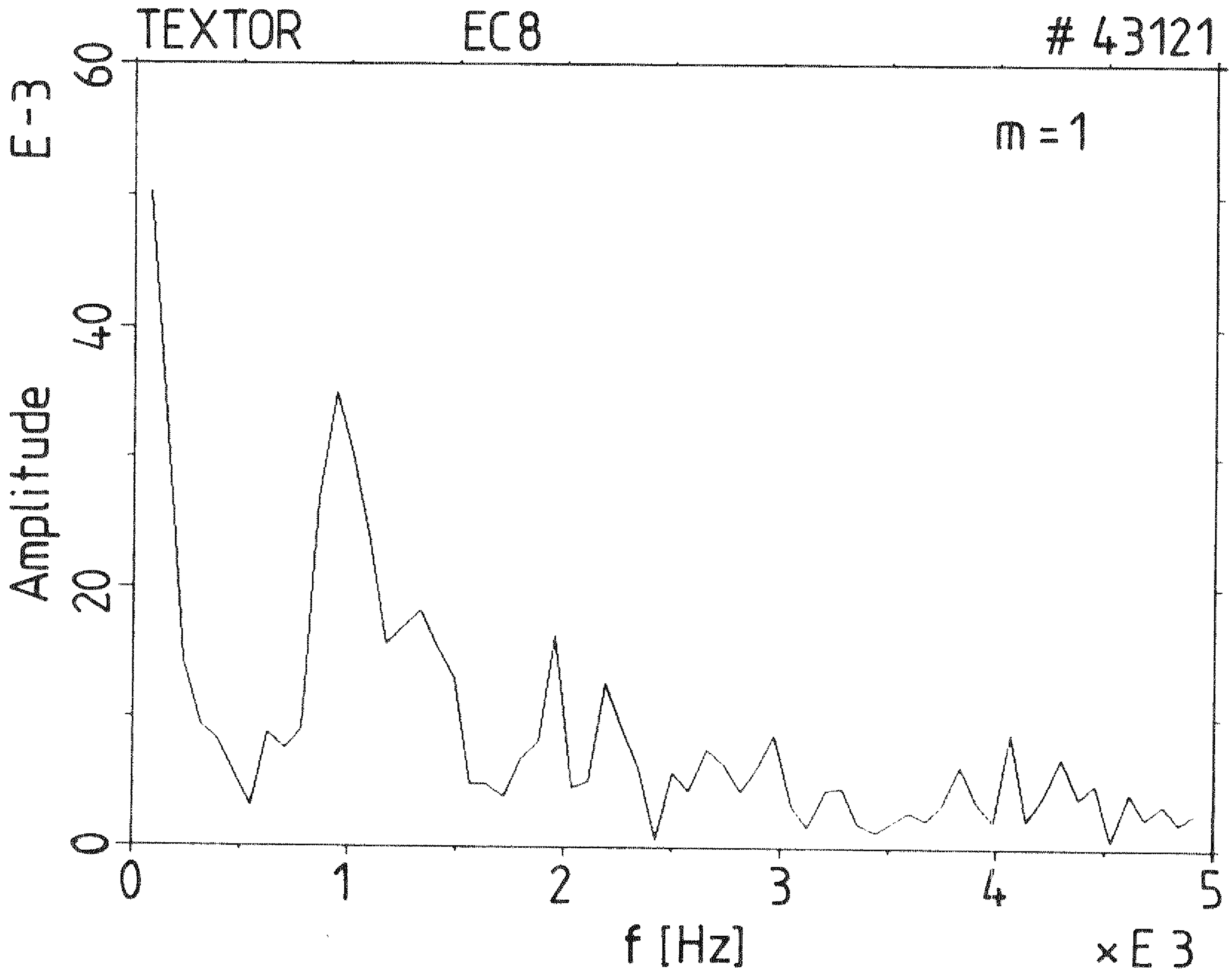

Fig. 8b

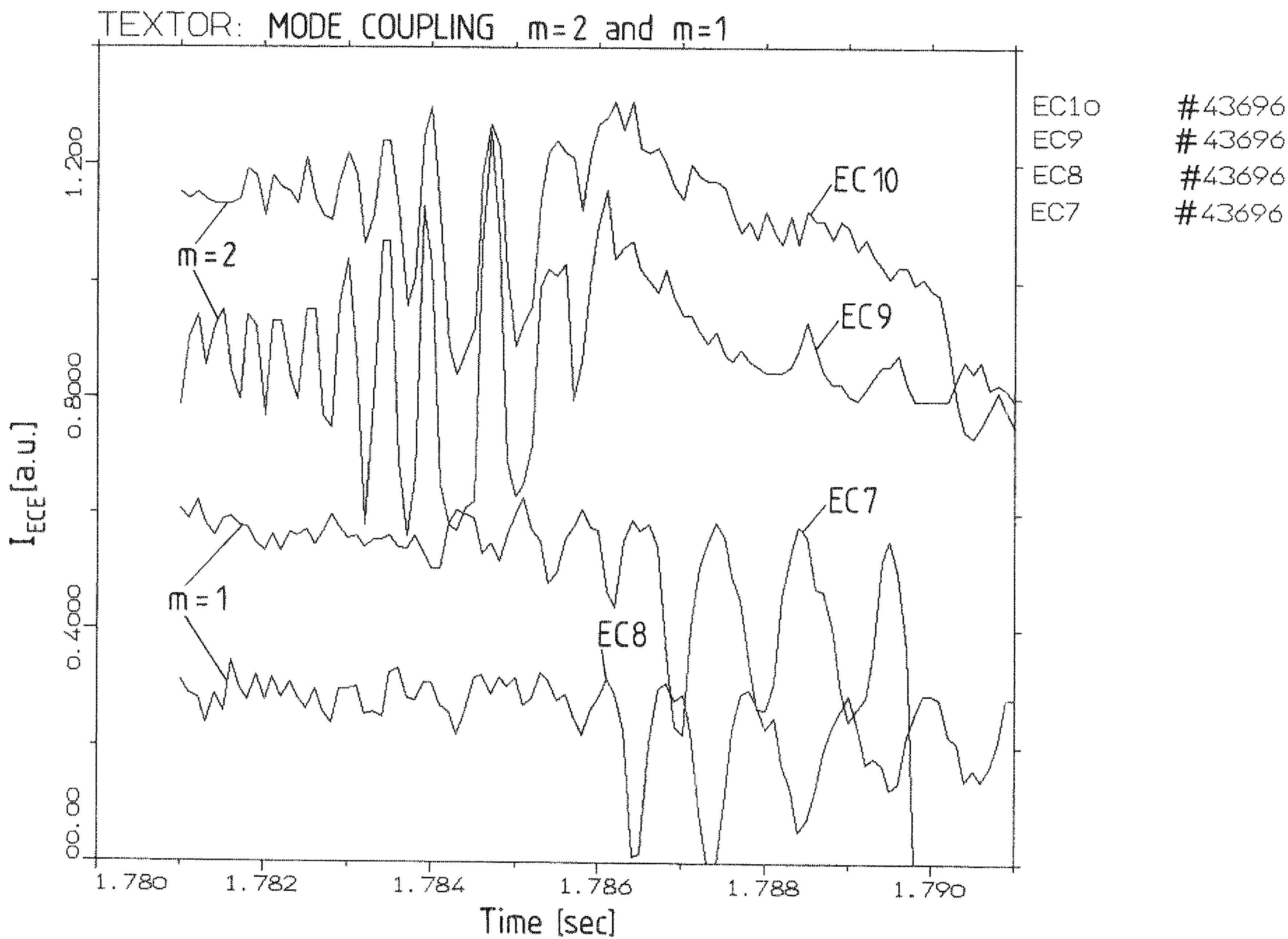
TEXTOR: MODE COUPLING m=2 and m=1
EC1o #43696
EC9 #43696
EC8 #43696
EC7 #43696
EC 10
EC9
EC7
EC8
m=2
m=1
I_ECE [a.u.]
1.200
0.8000
0.4000
00.00
1.780
1.782
1.784
1.786
1.788
1.790
Time [sec]

Fig. 9

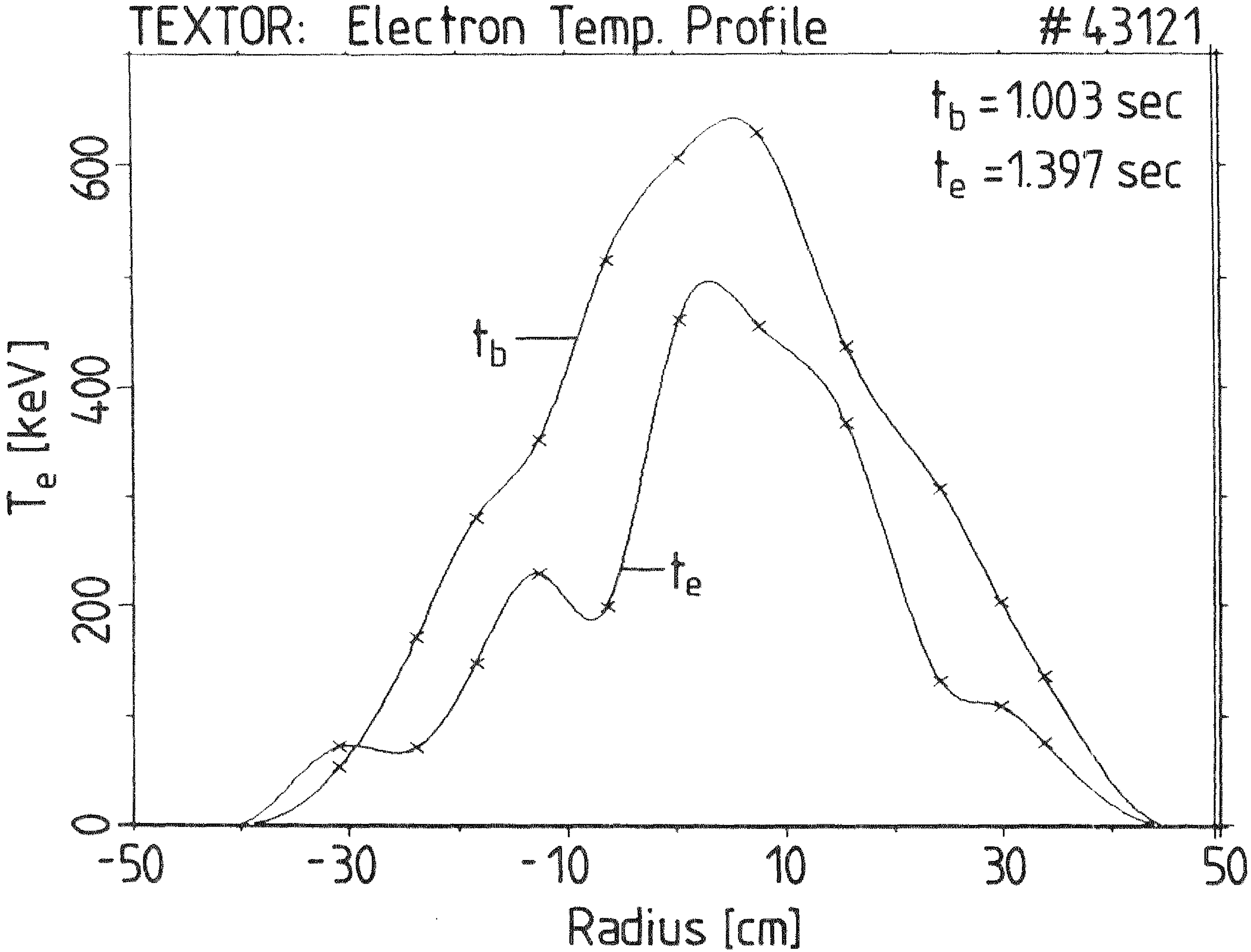

TEXTOR: Electron Temp. Profile
43121
t_b = 1.003 sec
t_e = 1.397 sec
t_b
t_e
600
400
200
0
T_e [keV]
-50
-30
-10
10
30
50
Radius [cm]

Fig. 10

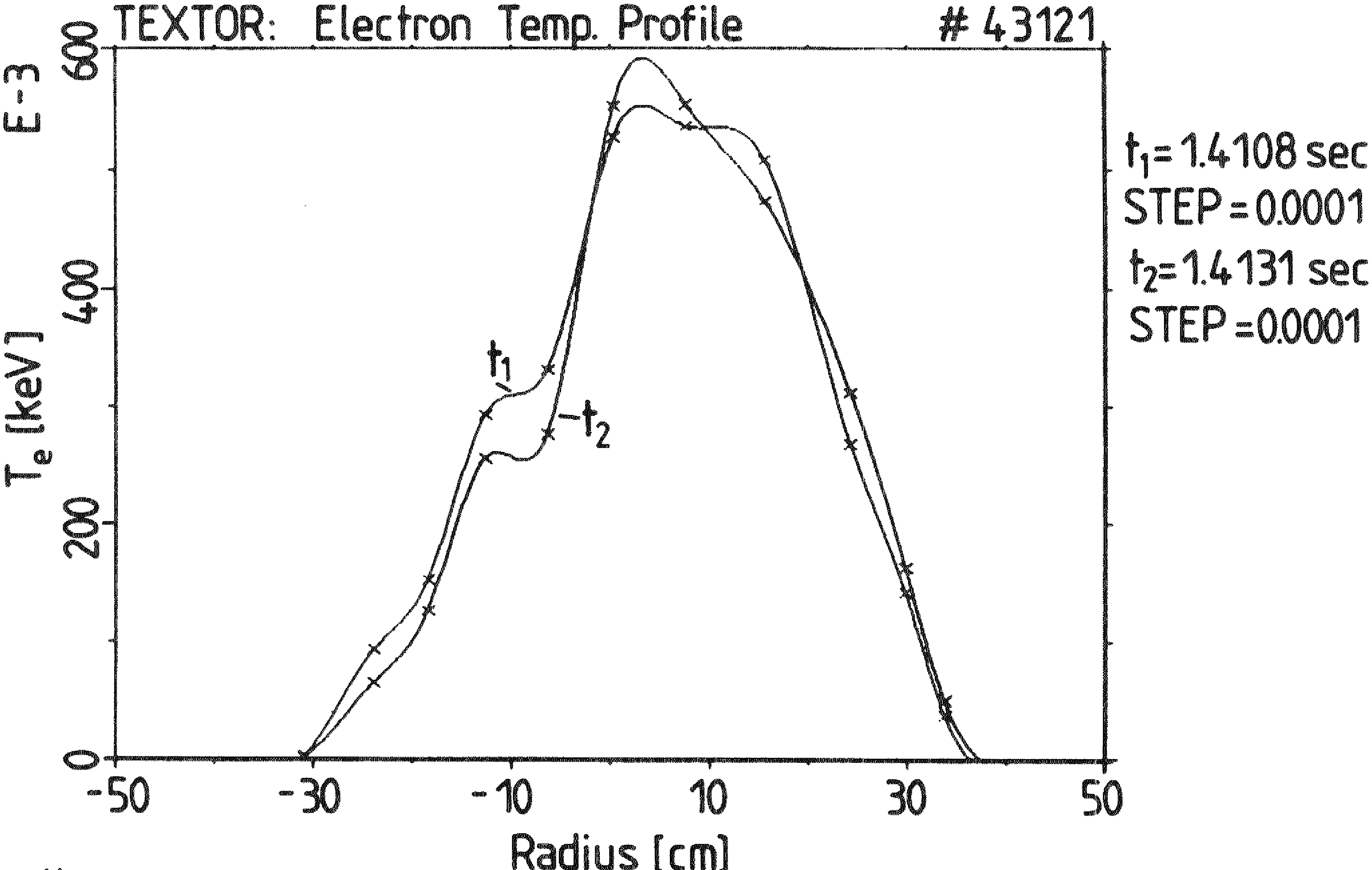
TEXTOR: Electron Temp. Profile
43121
E-3
600
400
200
0
Te [keV]
t1
t2
-50
-30
-10
10
30
50
Radius [cm]
t1= 1.4108 sec
STEP = 0.0001
t2= 1.4131 sec
STEP = 0.0001

Fig. 11

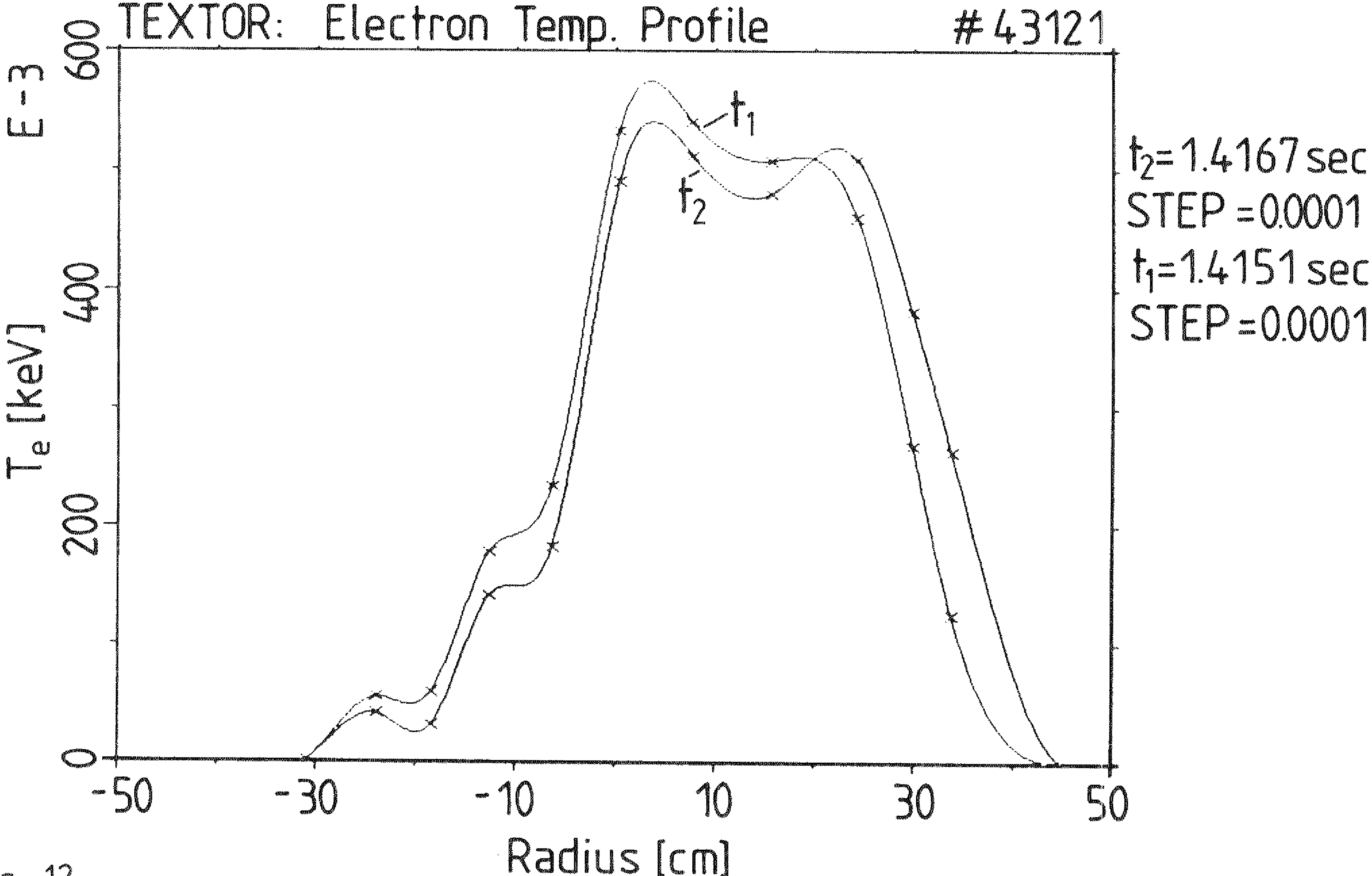
TEXTOR: Electron Temp. Profile
43121
E-3
Te [keV]
600
400
200
0
-50
-30
-10
10
30
50
Radius [cm]
t1
t2
t2= 1.4167 sec
STEP = 0.0001
t1=1.4151 sec
STEP = 0.0001

Fig. 12

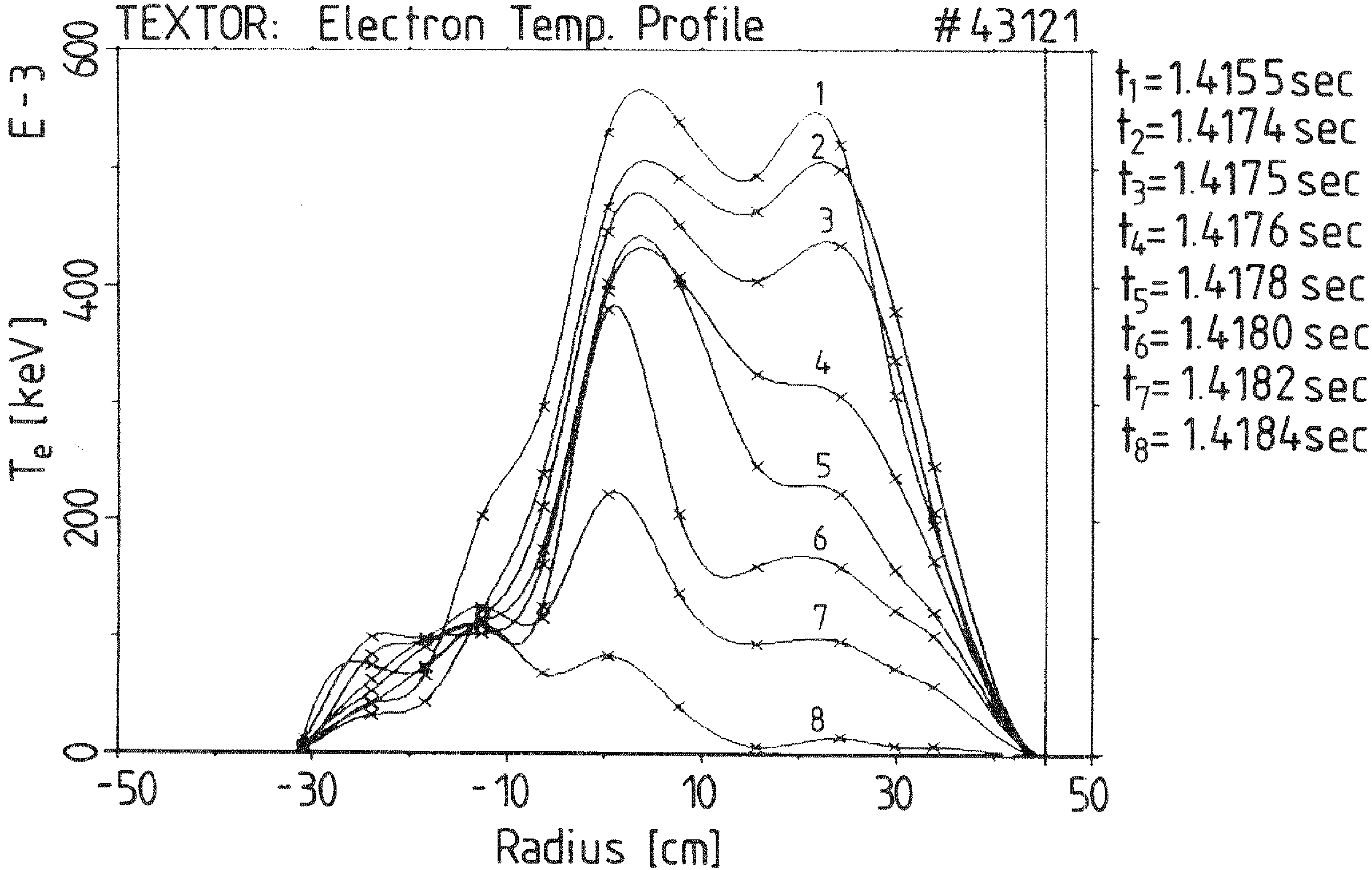

TEXTOR: Electron Temp. Profile
#43121
E-3
T_e [keV]
0
200
400
600
-50
-30
-10
10
30
50
Radius [cm]
1
2
3
4
5
6
7
8
t_1=1.4155 sec
t_2=1.4174 sec
t_3=1.4175 sec
t_4=1.4176 sec
t_5=1.4178 sec
t_6=1.4180 sec
t_7=1.4182 sec
t_8=1.4184 sec

Fig. 13

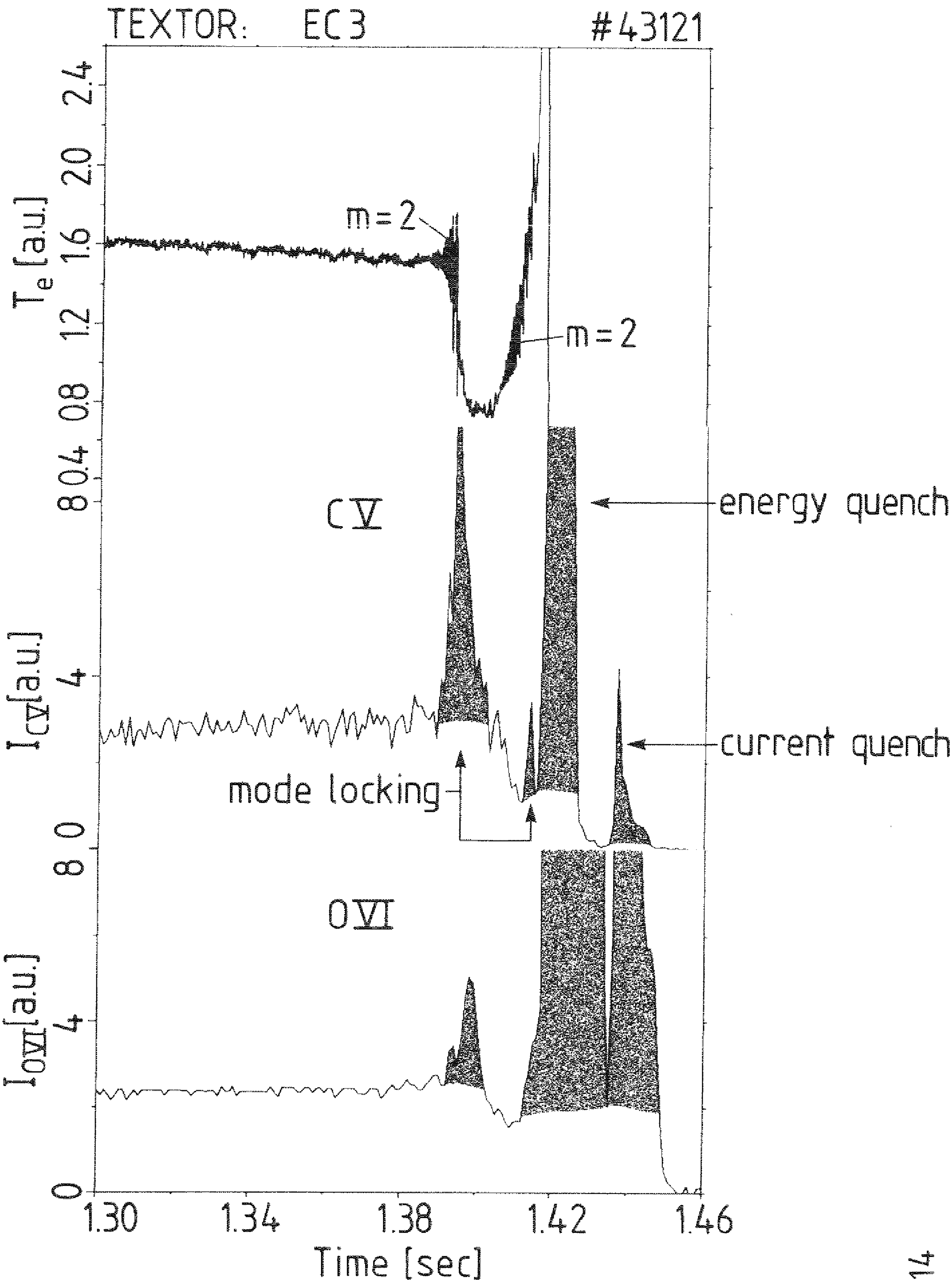
TEXTOR: EC3
#43121
T_e [a.u.]
m = 2
m = 2
C V
energy quench
I_CV [a.u.]
current quench
mode locking
O VI
I_OVI [a.u.]
Time [sec]

Fig. 14

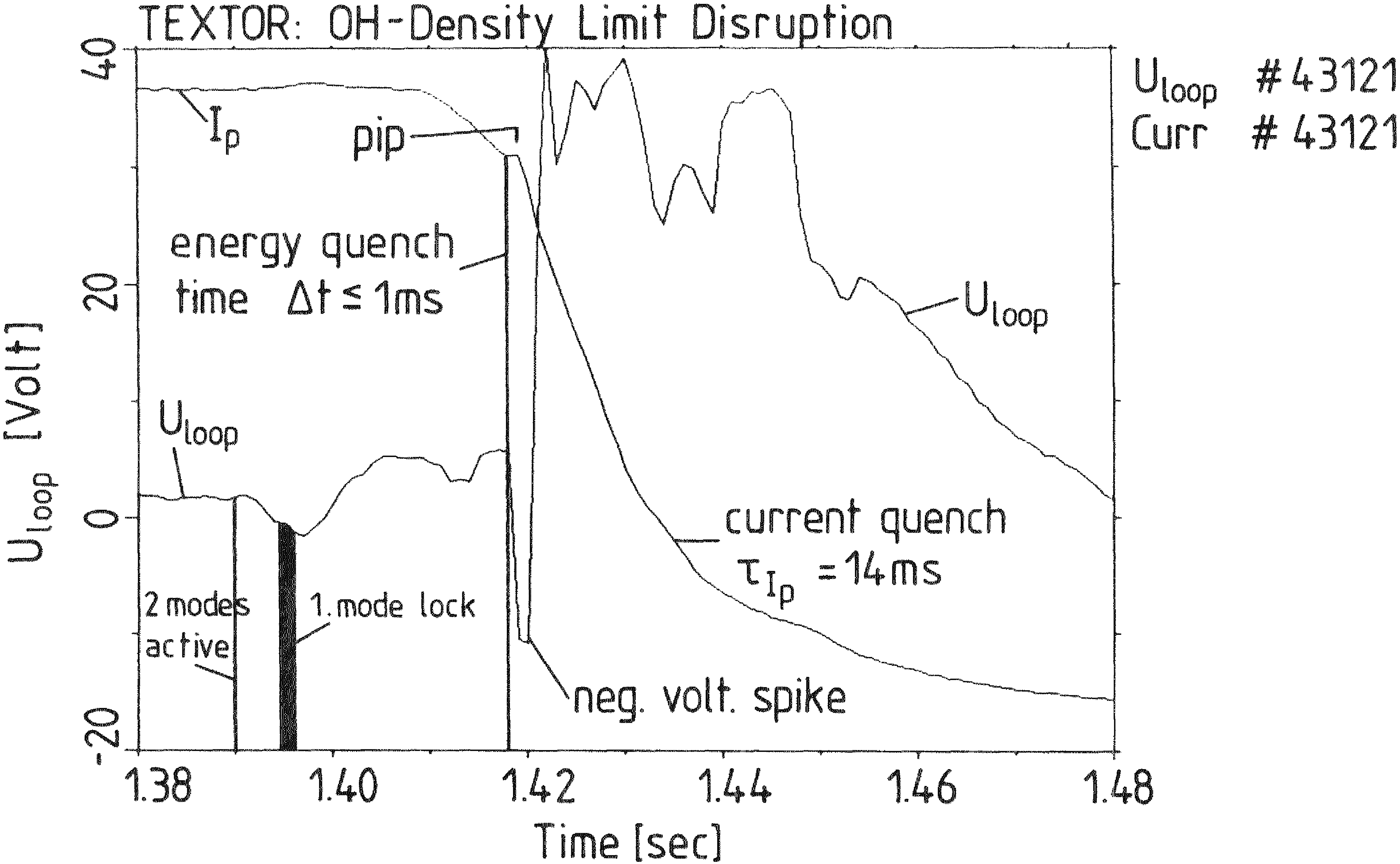

TEXTOR: OH-Density Limit Disruption
U_loop #43121
Curr #43121
I_p
pip
energy quench
time Δt ≤ 1ms
U_loop
U_loop
current quench
τ_Ip = 14ms
2 modes
active
1. mode lock
neg. volt. spike
U_loop [Volt]
40
20
0
-20
1.38
1.40
1.42
1.44
1.46
1.48
Time [sec]

Fig. 15

FORSCHUNGSZENTRUM JÜLICH GmbH

KFA

Jül-2448
Februar 1991
ISSN 0366-0885